Visual Motion Imagery Classification with Deep Neural Network based on Functional Connectivity

Byoung-Hee Kwon, Ji-Hoon Jeong, and Seong-Whan Lee*, *Fellow, IEEE*

***Abstract*—Brain-computer interfaces (BCIs) use brain signals such as electroencephalography to reflect user intention and enable two-way communication between computers and users. BCI technology has recently received much attention in healthcare applications, such as neurorehabilitation and diagnosis. BCI applications can also control external devices using only brain activity, which can help people with physical or mental disabilities, especially those suffering from neurological and neuromuscular diseases such as stroke and amyotrophic lateral sclerosis. Motor imagery (MI) has been widely used for BCI-based device control, but we adopted intuitive visual motion imagery to overcome the weakness of MI. In this study, we developed a three-dimensional (3D) BCI training platform to induce users to imagine upper-limb movements used in real-life activities (picking up a cell phone, pouring water, opening a door, and eating food). We collected intuitive visual motion imagery data and proposed a deep learning network based on functional connectivity as a mind-reading technique. As a result, the proposed network recorded a high classification performance on average (71.05%). Furthermore, we applied the leave-one-subject-out approach to confirm the possibility of improvements in subject-independent classification performance. This study will contribute to the development of BCI-based healthcare applications for rehabilitation, such as robotic arms and wheelchairs, or assist daily life.**

***Index Terms*—Brain-computer interface, electroencephalography, visual motion imagery, functional connectivity, deep learning**

I. Introduction

BRAIN-COMPUTER INTERFACE (BCI) is a technology that enables two-way communication between machines and users by using brain signals that reflect human intention. Non-invasive BCI is a practical method because no surgical operation is required [1], [2]. Electroencephalography (EEG) has the advantage of higher time resolution than comparable methods such as functional magnetic resonance imaging and near-infrared spectroscopy. Because EEG has the advantage of higher time resolution, it is possible to carry out fast communication between users and computers. These fast communications contribute to the development of rehabilitation systems for patients with tetraplegia or to supporting the daily life activities of healthy people [3]–[5].

This research was supported by an Institute of Information & Communications Technology Planning & Evaluation (IITP) grant, funded by the Korean government (No. 2017-0-00432; No. 2017-0-00451; No. 2019-0-00079).

B.-H. Kwon and J.-H. Jeong are with the Department of Brain and Cognitive Engineering, Korea University, Anam-dong, Seongbuk-ku, Seoul 02841, South Korea. E-mail: bh_kwon@korea.ac.kr, jh_jeong@korea.ac.kr.

S.-W. Lee is with the Department of Artificial Intelligence, Korea University, Anam-dong, Seongbuk-ku, Seoul 02841, South Korea. E-mail: sw.lee@korea.ac.kr.

*S.-W. Lee is the corresponding author.

Traditional EEG-based BCI applications are controlled by using mind-reading technology or decoding user intention [6]–[11]. EEG-based BCI technologies are commonly used in healthcare applications ranging from prevention, detection, and diagnosis to rehabilitation and restoration [12]–[15]. Extensive BCI research is being conducted specifically to develop devices to help people with disabilities who are affected by neurological and neuromuscular conditions, such as spinal cord injury, amyotrophic lateral sclerosis, and strokes. For example, people with paraplegia or other movement disorders can use an EEG-assisted BCI device to drive a wheelchair [8], [16] or to control a robotic arm [2], [3], [10], [17]. In addition, the evaluation of brain signals using EEG helps to treat neurological disorders such as migraine and cluster headache and may play an important role in neural prostheses [18].

Previous studies utilized a variety of BCI paradigms to identify users' intent to move. BCI paradigms are sorted into exogenous and endogenous paradigms according to the type of stimulation and imagination. The paradigms, which are based on external stimuli such as steady-state visual evoked potentials [6], [8] and event-related potential [9], are known as exogenous BCIs. The exogenous BCI paradigm has the advantages of rapid response time and high accuracy, but it also has the disadvantage of requiring external devices. On the other hand, the endogenous BCI paradigm has the disadvantages of being slow in response and less accurate than the exogenous paradigm, but it does not require stimulation from external devices and allows users to use their voluntary intentions. Among the endogenous BCI paradigms, motor imagery (MI) [2], [10], [19]–[21] is an effective option for controlling practical BCI applications such as robotic arms or wheelchairs. When a user performs motor imagery, event-related desynchronization/synchronization (ERD/ERS), referred to as sensory-motor rhythm, is generated in the motor cortex [17]. ERD/ERS can be induced from the mu band [8–12 Hz] and beta band [13–30 Hz], respectively.

Although the MI paradigm is widely used in BCI studies, imagining muscle movements is not intuitive for users. Although a user imagines the same muscle movement when performing the MI paradigm, it is difficult to detect the user's intentions because the time and sequence of imagery in which the user imagines muscle movements are not constant. In addition, MI is accepted differently by users, and this phenomenon prevents users from having a uniform imagination [22]–[25]. This leads to motion-related signals in different brain regions for each person and degrades the practicality of BCI applications. To overcome this limitation, in this study, we

adopted visual motion imagery as an intuitive BCI paradigm.

Visual imagery is an endogenous BCI paradigm that allows users to imagine more intuitively than MI when a user performs imagery tasks [26]. Visual imagery can be performed intuitively regardless of the complexity of movement, reducing the difficulty of imagination and reducing the fatigue that users receive. To decode user intention, we used neural response patterns that include delta, theta, and alpha frequency bands. Brain activities based on visual imagery induce the delta and theta bands in the prefrontal lobe and the alpha band in the occipital lobe, which includes the visual cortex [27].

In this study, visual motion imagery, an advanced BCI paradigm of visual imagery [27], [28], was used to provide more intuitive stimuli to users. Visual motion imagery is a paradigm that uses moving scenes to provide stimulation, unlike conventional visual imagery that provides static stimulation. We provided visual stimuli in a three-dimensional (3D) virtual environment for users to effectively perform visual motion imagery. The visual motion imagery paradigm that we designed presented the high-complexity upper limb movement stimulation required by the user to help the user intuitively perform imaginary tasks. In addition, it is possible to obtain the effect of training a user by repeatedly providing 3D visual stimuli. Hence, mind-reading could be performed effectively to obtain accurate brain signals. Visual motion imagery allows users to perform more advanced tasks when performing BCI-based device control because the user is given a moving stimulus.

We proposed a deep learning framework based on functional connectivity and a convolutional neural network (CNN)-bidirectional long short-term memory (BiLSTM) network to facilitate the robust decoding of visual motion imagery. We classified brain signals derived from humans when imagining four kinds of motions (picking up a cell phone, pouring water, opening a door, and eating food) and evaluated the performance using our network that considers both spatial and temporal information.

The contributions of this study can be divided into three parts. (*i*) EEG data that can provide more useful movements to users is collected using a 3D visual motion imagery paradigm with high complexity. (*ii*) We proposed a functional connectivity-based deep neural network to decode visual motion imagery from subjects. Because a certain spatial pattern is found in visual motion imagery, our proposed network emphasizes spatial information based on the phase-locking value (PLV) for robust decoding performance. (*iii*) For practical use of BCI-based healthcare applications, the possibility of robust classification in the subject-independent condition was investigated by applying a leave-one-subject-out (LOSO) approach.

II. Materials and Methods

A. Participants

Fifteen subjects (Sub1-Sub15; aged 20–30 years) who had no neurological disease participated in our experiments. The subjects were asked to avoid anything that could affect physical and mental conditions for the experiment, such as drinking alcohol or having psychotropic drugs before the experiment day. In addition, participants were instructed to sleep for more than 8 h the day before the experiment for their condition. This study was reviewed and approved by the Institutional Review Board at Korea University (KUIRB-2020-0013-01), and written informed consent was obtained from all participants before the experiment.

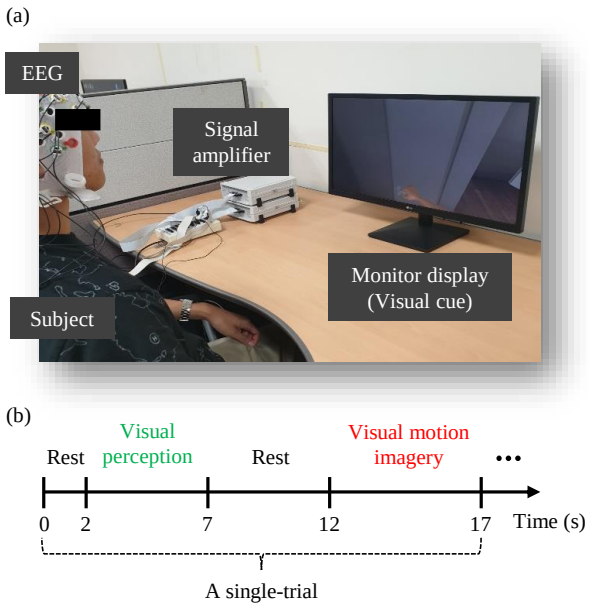

Fig. 1. Experimental protocols for visual motion imagery from electroencephalography (EEG) signals (a) Experimental environment to acquire visual motion imagery data. (b) Experimental paradigm in a single trial and representation of visual cues according to each task.

B. Data Acquisition

EEG data were recorded using an EEG signal amplifier (BrainAmp, Brain Products GmbH, Gilching, Germany) with MATLAB 2019a (MathWorks, Natick, MA), sampled at 1,000 Hz. Additionally, we applied a 60-Hz notch filter to reduce the effect of external electrical noises (e.g., direct-current noise due to power supply, the scan rate of the monitor display, and frequency of the fluorescent lamp) in the raw signals. EEG was recorded from 64 Ag/AgCl electrodes according to the International 10–20 system (Fp1-2, AF5-6, AF7-8, AFz, F1-8, Fz, FT7-8, FC1-6, T7-8, C1-6, Cz, TP7-8, CP1-6, CPz, P1-8, Pz, PO3-4, PO7-8, POz, O1-2, Oz, and Iz). The ground and reference channels were placed on Fpz and FCz, respectively. To maintain the impedance between the electrodes and skin below 10 kΩ, we injected conductive gel into the electrodes using a syringe with a blunt needle. A display monitor to provide the experimental paradigm to the subject was placed at a distance of approximately 90 cm for a comfortable state for the subject, and the subject sat in a comfortable position to conduct the experiment, as shown in Fig. 1(a).

C. Experimental Paradigm

As shown in Fig. 1(b), a single trial in the experimental paradigm was designed to include four different phases. The

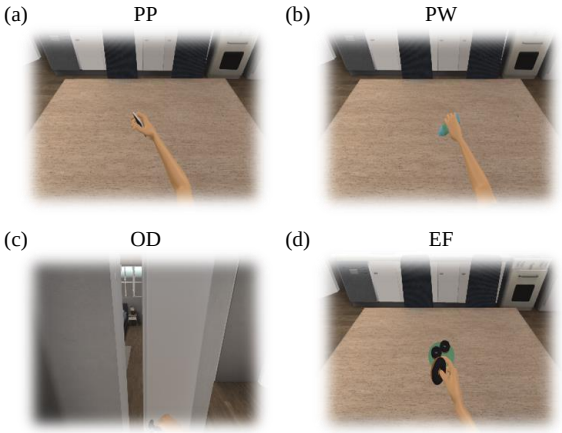

Fig. 2. The representation of classes provided to the subjects as stimuli during visual motion imagery experiment. The classes consist of four types: (a) picking up a cell phone (PP), (b) pouring water (PW), (c) opening a door (OD), and (d) eating food (EF).

first phase is a resting state that presents a fixation cross on the screen to provide a comfortable environment to the subjects for 2 s before providing the visual motion stimuli. The visual motion stimuli that subjects should imagine were given in the second phase as a visual cue. The third phase is another resting state with a fixation cross that provides sufficient time to remove the afterimage of the stimulus in the second stage for 5 s. This stage is essential to obtain clear and meaningful EEG data from the visual motion imagery stage. In the fourth stage, after the 5-s resting phase, the subjects performed the visual motion imagery for 5 s based on the visual cues provided in the second stage. During the visual motion imagery, the subjects saw a blank screen with their eyes open and imagined drawing a scene over the screen. The duration of a single trial that consisted of all the four stages mentioned above was 17 s long, and the subject performed 50 trials in each class, for a total of 200 trials. The subjects received trials of each class in random order. As a result, 200 trials were conducted for each subject.

We designed a 3D moving visual stimulation that we called the 3D-BCI training platform as a guide to the experimental protocols. These stimuli provide guidance on what the subject should imagine. The subjects performed visual motion imagery based on a given visual cue. We used 3D simulation software such as Unity 3D (Unity Technologies, San Francisco, CA) and Blender (Blender 3D Engine: www.blender.org) to design videos that were presented to the subjects. As shown in Fig. 2, the visual stimuli consisted of four different scenarios: picking up a cell phone (PP), pouring water (PW), opening a door (OD), and eating food (EF). The classes were designed based on movements that the user could perform in real life. In this manuscript, we defined three different complexity cases as follows: 2-class (PW/EF), 3-class (PW/OD/EF), and 4-class (PP/PW/OD/EF).

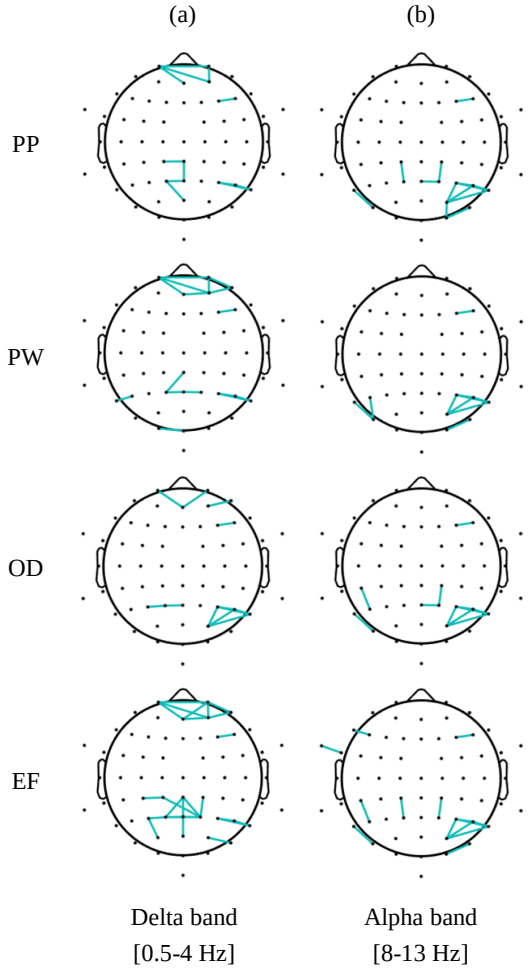

Fig. 3. The selected channel connections using functional connectivity have a correlation score above 0.9. Functional connectivity was applied in the delta and alpha frequency ranges. In the delta frequency range, connections are represented in the prefrontal lobe. In the alpha frequency range, the connections were mainly represented in the occipital lobes, regardless of class.

D. Pre-processing

The EEG data were pre-processed using the BBCI toolbox in a MATLAB 2019a environment. Raw EEG data were down-sampled from 1,000 to 250 Hz. We applied a band-pass filter between 0.5–13 Hz using Hamming-windowed zero-phase finite-impulse response filters with an optimized order (N = 30), including the delta, theta, and alpha band frequencies that are related to visual motion imagery [27]. We set the sliding window length to 2 s with 50% overlap as an augmentation method to increase the number of training data for the deep learning network. The data of each subject consisted of 800 samples, and we randomly selected 80% of the trials as a training set and 20% as a test set for adopting leave-one-out cross-validation.

E. Functional Connectivity based Deep Neural Network (FuDNN)

Functional connectivity is a method used to assess neural interactions [29]. We utilized functional connectivity as a method to evaluate regional interactions that occur in the brain

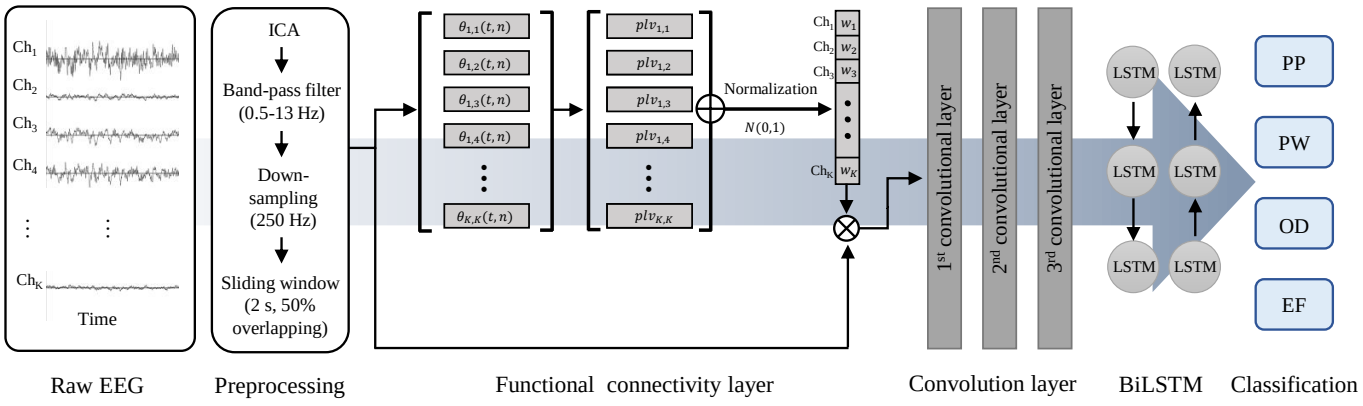

Fig. 4. The overview of the proposed architecture. In the functional connectivity layer, the raw electroencephalogram (EEG) will be channel-wise multiplied using a functional connectivity score measured by the phase-locking value. The modified EEG data that emphasize spatial information becomes the input data of the deep learning architecture. We extracted spatial information using a network consisting of convolution layers, followed by temporal information via bidirectional long short-term memory layers (BiLSTM).

when a subject performs visual motion imagery. We selected the PLV method [30], [31] as a functional connectivity method to calculate the relation score of each channel.

Human brain signals can be expressed by correlations between brain regions. In order to decode user intention, applying raw EEG signals that do not reflect correlations between regions of the brain and the deep neural network leads to performance degradation. Therefore, we measured the functional connectivity score using PLVs to consider the spatial positional relationship. As shown in Fig. 3, we visualized the functional connectivity of the topography when the subjects performed the visual motion imagery in each class to see if this method was appropriate for decoding the visual motion imagery. In this study, we identified the functional connectivity in all classes using the delta [0.5-4 Hz] and alpha [8–13 Hz] frequency ranges in which the significant features appear in the visual motion imagery. As a result, there are strong correlations in delta regions, mainly near the prefrontal lobe (Fig. 3(a)), and in the alpha frequency range, mainly near the occipital lobe (Fig. 3(b)). These results show the same tendency regardless of class, which demonstrates that applying PLVs to decode the visual motion imagery is reasonable.

In this study, we proposed a functional connectivity-based deep neural network (FuDNN) to decode acquired visual motion imagery data. An overview of the proposed FuDNN is presented in Fig. 4, and the architecture design is presented in Table I. As the first step of FuDNN, we reconstructed the raw EEG signal as an input to the deep learning network using functional connectivity. First, we denote the format of the functional connectivity layer as

$$PLV = \{plv_{k_1,k_2} \mid 1 \le k_1 \le K, 1 \le k_2 \le K\}, \quad (1)$$

where k_1 and k_2 are the channels in which we compare the phase, and K is the number of all electrodes used. The phase of this convolution $\phi_{k_1}(t,n)$ is extracted for all time bins t and trial n $[1,...,N]$, and the phase difference between k_1 and k_2 is derived from $\theta(t,n) = \phi_{k_1}(t,n) - \phi_{k_2}(t,n)$.

TABLE I
DESCRIPTION OF THE PROPOSED FUDNN ARCHITECTURE

Layer	Type	Parameter	Output size
1	Input	-	1 × 64 × 500
2	Convolution	Filter size: 1 × 50 Stride size: 1 × 1 Feature map: 40	40 × 64 × 451
	BatchNorm	-	
3	Convolution	Filter size: 1 × 50 Stride size: 1 x 1 Feature map: 40	80 × 64 × 402
	BatchNorm	-	
	Activation (ELU)	-	
4	Average pooling	Filter size: 1 × 7 Stride size: 1 × 7 Dropout (0.5)	80 × 64 × 57
5	Depthwise separable convolution	Filter size: 64 × 1 Stride size: 1 x 1	80 × 1 × 57
	BatchNorm	-	
	Activation (ELU)	-	
6	Average pooling	Filter size: 1 × 7 Stride size: 1 × 7 Dropout (0.5)	80 × 1 × 8
7	BiLSTM	Hidden units: 100	8 × 200
8	Fully connected	-	1 × 1600
9	Softmax	-	1 × 4

$$plv_{k_1,k_2} = \frac{1}{NT}\sum_{t=1}^{T}\sum_{n=1}^{N} e^{j\theta(t,n)} \quad (2)$$

These formulas can be used to understand the correlation between channels and to emphasize the spatial information in raw EEG signals. plv_{k_1,k_2} obtained from the above formula is an upper triangular matrix, so it was transposed to create a lower triangular matrix, and adding the two matrices to create a new matrix S_{k_1,k_2} in the form of a symmetric matrix.

$$S_{k_1,k_2} = plv_{k_1,k_2} + (plv_{k_1,k_2})^T \quad (3)$$

To emphasize the spatial information in the input signal, we transformed the previously obtained S_{k_1,k_2} into a matrix of 1 × K using the following formula:

$$\widetilde{PLV} = \sum_{k_1=1}^{K} S_{k_1,k_2} \tag{4}$$

We limited the distribution of $P\tilde{L}V$ between 0 and 1 using the simplest method, min-max normalization, to emphasize channels using $P\tilde{L}V$ implemented in one dimension.

$$w_K = \frac{\widetilde{PLV_K} - \widetilde{PLV_{min}}}{\widetilde{PLV_{max}} - \widetilde{PLV_{min}}}. \tag{5}$$

This result is that of the 64 channels, the value of the channels that are highly correlated with the visual motion imagery is close to 1, and the channels that do not correlate have a value close to zero. w_K is a weight that emphasizes spatial information using channels related to visual motion imagery in the proposed network. The channel axis of the pre-processed EEG signal is multiplied by w_K, and the data are reconstructed according to the degree of visual motion imagery.

Conventional EEG-related deep learning frameworks use CNNs to train spatial features [32]–[34] and use LSTM to train temporal features [35]–[37]. Based on these studies, we used CNN in our proposed network to extract spatial information with spatially focused data using PLVs. When features are extracted via reconstructed EEG data using PLVs, the effect of emphasizing the channel that is most affected when performing visual motion imagery is greater than that of extracting features using raw EEG data. The first and second convolutional layers were designed to handle all electrode channels. In this stage, each layer performs spatial filtering with the weights listed in Table I. Batch normalization was applied to standardize the variance of the learned data. Because the first convolutional layer did not improve performance even with non-linear activation, we designed the network to maintain linearity without using the activation function in the first layer. In the second convolutional layer, we applied exponential linear units (ELUs) [38] as an activation function. After two convolutional layers, we used an average pooling layer to resize the convolution, which had a 1×7 kernel size with a stride of 1×7. In addition, we set the dropout probability to 0.5, after the average pooling layer, to help prevent the overfitting problem that occurred during training on small sample sizes. Then, we used a depth-wise separable convolution layer [39], [40] with the parameters shown in Table I to reduce the number of trainable features and to decouple the relationship within and across feature maps. The output of the second average pooling layer becomes an input feature of the BiLSTM network [41], [42]. In this manner, the BiLSTM network extracted features based on temporal information using spatially trained features. Finally, the features are fed into the softmax classifier, and we used the categorical cross-entropy loss function with the Adam optimizer.

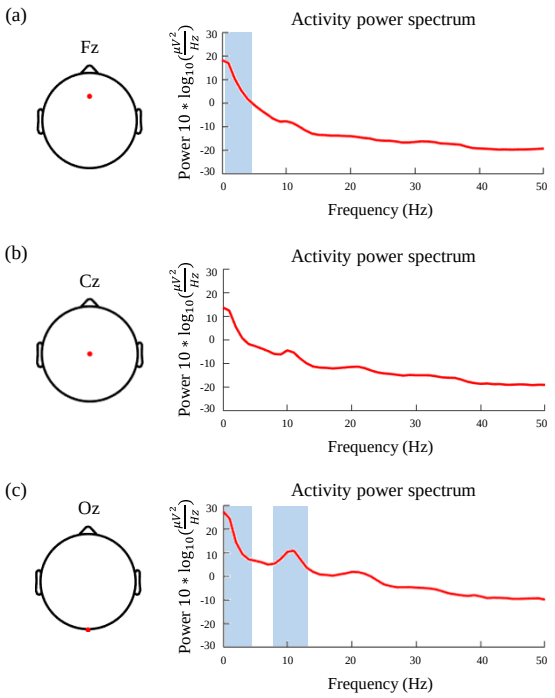

Fig. 5. The power spectral changes in each selected channel. The blue box in the graph indicates the frequency range containing a significant peak. The peaks were observed in channels (a) Fz and (c) Oz related to visual motion imagery, and low-power spectral changes were observed in channel (b) Cz that was not related to visual motion imagery.

III. Experimental Results

A. Data Analysis

We used the BBCI toolbox [43] and EEGLab toolbox [44] (version 14.1.2b) to verify the quality of the collected EEG data. The BBCI toolbox was used to measure the magnitude of the power of the visual motion imagery data for each frequency range in each area of the brain. We used imagery data for each stimulus as visual motion imagery data and used 0-5 s corresponding to the entire interval of the visual motion imagery phase. Among the 64 channels, Fz representing the prefrontal lobe, Cz representing the motor cortex, and Oz representing the occipital lobe were selected to measure the power spectral changes from 0.1-50 Hz in each selected channel. The frequency-specific power measured at each channel determines which area of the brain is significant when performing visual motion imagery. While the user performed visual motion imagery, there were significant changes in brain-signal power that occurred on channels representing the prefrontal and occipital lobes. A delta power peak is observed on the Fz channels (Fig. 5(a)), while delta power and alpha power peaks are found on the Oz channels (Fig. 5(b)). On the other hand, no significant peak could be observed in any frequency range on the Cz channel (Fig. 5(c)), which proves that the visual motion imagery-related brain signal did not occur in the motor cortex, and the acquired EEG signal corresponded to pure visual motion imagery.

Subsequently, we measured the variation in the spectral

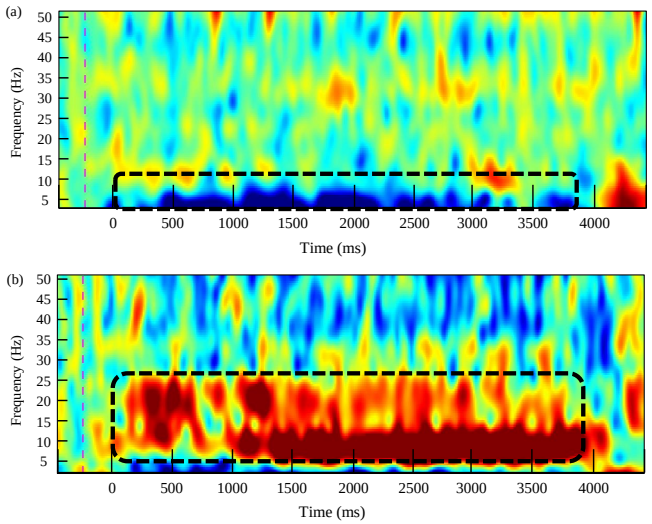

Fig. 6. Event-related spectral perturbation representation of visual motion imagery in the selected channels. The red dotted line indicates the beginning of the baseline. Significant activation was observed in the delta wave between 0.5-4 Hz in (a) the Fz channel and between 8-13 Hz in (b) the Oz channel.

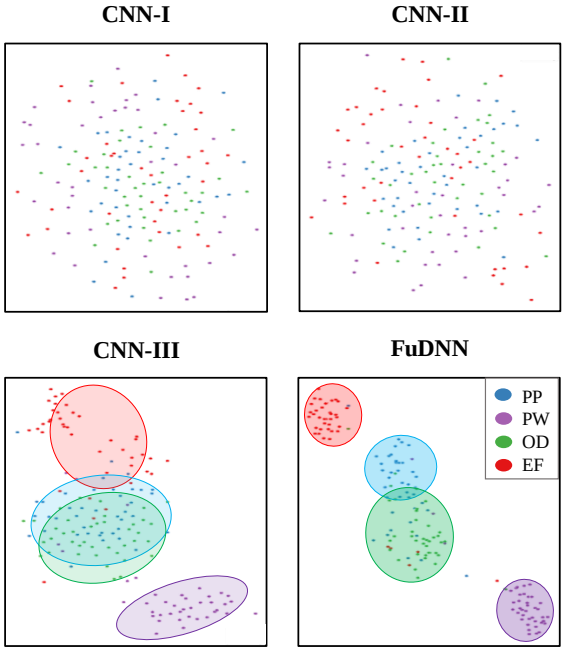

Fig. 7. Representations of visualized feature distribution in each layer using t-distributed stochastic neighbor embedding (t-SNE). The more layers of the network are added, the clearer the clustering of the feature distribution in each class. In addition, the clearest feature distribution can be observed when all the proposed networks are used. CNN, convolutional neural network; FuDNN, functional connectivity-based deep neural network.

power of visual motion imagery based on the event-related spectral perturbation (ERSP) method [44], [45] on two channels that are considered to be related to visual motion imagery. ERSP analysis was performed between 0.5-50 Hz, using 400 timepoints. The baseline was set from -500 to 0 ms before the visual motion imagery phase in order to analyze the phenomena when subjects imagined an action. From the above results, it can be inferred that visual motion imagery exhibits strong brain-signal features in the prefrontal and occipital lobes. Accordingly, we measured ERSP on Fz and Oz, two channels related to the visual motion imagery mentioned above. As shown in Fig. 6, Fz, which represents the prefrontal lobe, shows a strong activity power spectrum in the delta wave, and Oz, which represents the occipital lobe, shows a strong activity power spectrum in the alpha wave.

B. Ablation Study

In this work, we proposed FuDNN, which is a robust classification method for EEG signal variability. To validate the ability of the proposed network, we visualized the output features of each layer using the t-distributed stochastic neighbor embedding (t-SNE) method [49], [50]. Fig. 7 shows the distribution of the features of a test set at the outputs of each significant layer. The more we used the overall structure of the proposed network, the more obvious the clustering distribution of the output features. These results indicate an increase in the classification performance, and to verify these results, we derived the classification performance with an ablation study using each layer.

CNN-I is a network that contains only the first convolution layer of the proposed network. CNN-II is composed of two convolutional layers and includes layers 1 and 2, as shown in Table I. CNN-III includes layers 1 to 5 represented in Table I. Finally, FuDNN stands for the entire network proposed in this paper. As shown in Fig. 9, we found that classification

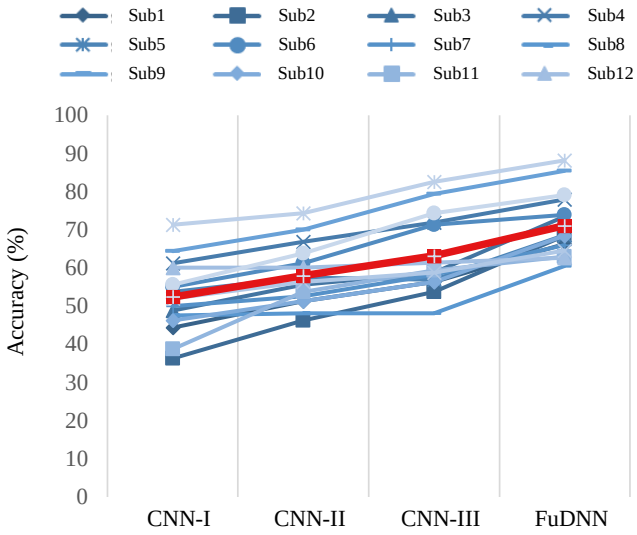

Fig. 8. The graph representation of classification performance by subject in each layer. The red line corresponds to the average classification performance of all the subjects. The more layers are added, the higher the classification performance. CNN, convolutional neural network; FuDNN, functional connectivity-based deep neural network.

performance increases as networks become more similar to those proposed in this study. The average classification performances at each layer were 52.34%, 57.92%, 63.13%, and 71.05%, respectively, with the largest difference in classification performance between CNN-II and CNN-III. These results

TABLE II
THE COMPARISON OF CLASSIFICATION PERFORMANCE WITH CONVENTIONAL METHODS

Subjects	2-class				3-class				4-class			
	CSP [46]	DeepConvNet [47]	EEGNet [48]	FuDNN	CSP [46]	DeepConvNet [47]	EEGNet [48]	FuDNN	CSP [46]	DeepConvNet [47]	EEGNet [48]	FuDNN
Sub1	51.70% (±3.23)	91.00% (±2.00)	79.25% (±5.51)	92.50% (±2.09)	43.87% (±1.83)	70.66% (±2.80)	66.00% (±2.06)	71.17% (±1.55)	31.95% (±2.24)	60.37% (±2.25)	57.37% (±2.77)	66.25% (±1.12)
Sub2	57.60% (±4.14)	95.00% (±0.79)	67.25% (±2.00)	97.00% (±0.61)	35.20% (±2.48)	76.16% (±1.63)	57.83% (±5.83)	76.67% (±1.49)	26.15% (±1.13)	63.37% (±1.01)	50.75% (±5.44)	68.37% (±1.16)
Sub3	55.40% (±2.41)	97.00% (±1.87)	85.50% (±2.31)	97.50% (±1.36)	32.87% (±3.11)	80.66% (±3.30)	66.00% (±3.04)	85.33% (±1.35)	27.75% (±2.12)	68.50% (±1.56)	61.87% (±1.18)	73.50% (±0.94)
Sub4	62.40% (±2.17)	92.25% (±2.15)	88.50% (±2.55)	95.50% (±0.61)	68.00% (±1.96)	90.33% (±0.66)	83.50% (±0.62)	88.17% (±0.33)	49.50% (±2.09)	75.00% (±1.04)	73.25% (±2.06)	77.88% (±1.02)
Sub5	98.50% (±0.30)	92.00% (±1.27)	81.50% (±2.67)	94.75% (±0.50)	90.80% (±1.36)	78.33% (±1.90)	67.83% (±4.23)	84.83% (±0.81)	86.25% (±1.27)	63.75% (±1.89)	61.12% (±3.14)	68.50% (±0.64)
Sub6	52.10% (±4.38)	87.00% (±2.03)	77.00% (±0.61)	93.75% (±0.79)	50.47% (±3.31)	77.83% (±1.24)	69.50% (±1.87)	83.00% (±0.85)	28.20% (±1.42)	65.62% (±1.97)	58.37% (±1.15)	73.88% (±1.07)
Sub7	54.20% (±3.79)	90.50% (±1.00)	87.00% (±1.28)	90.75% (±1.27)	60.53% (±2.07)	79.33% (±2.55)	70.33% (±2.14)	80.00% (±2.23)	47.65% (±1.94)	62.37% (±1.64)	58.00% (±2.48)	66.00% (±1.15)
Sub8	52.70% (±3.05)	90.25% (±1.22)	83.25% (±2.03)	88.75% (±1.11)	43.07% (±2.59)	70.33% (±2.21)	61.67% (±2.93)	72.33% (±1.85)	32.65% (±2.24)	56.50% (±1.28)	52.00% (±3.31)	60.50% (±0.72)
Sub9	55.50% (±3.65)	96.75% (±1.00)	96.50% (±0.93)	99.50% (±0.61)	48.80% (±1.98)	88.50% (±0.97)	86.00% (±1.11)	91.00% (±0.62)	37.90% (±3.35)	83.37% (±1.22)	78.00% (±1.95)	85.38% (±0.63)
Sub10	50.40% (±2.27)	93.0% (±1.27)	79.75% (±2.69)	95.25% (±0.93)	35.47% (±2.77)	68.33% (±2.47)	58.83% (±2.96)	78.83% (±1.45)	28.65% (±1.42)	58.62% (±2.17)	51.75% (±0.72)	68.38% (±0.84)
Sub11	48.30% (±3.12)	89.75% (±1.83)	77.25% (±0.93)	91.00% (±1.45)	32.87% (±1.77)	79.33% (±1.43)	62.50% (±2.04)	82.50% (±1.39)	25.80% (±1.94)	60.37% (±1.87)	50.37% (±1.09)	62.88% (±0.93)
Sub12	51.10% (±2.55)	93.50% (±1.22)	90.75% (±2.69)	95.00% (±1.12)	42.53% (±1.78)	75.83% (±0.91)	71.50% (±2.49)	79.17% (±1.17)	38.45% (±2.24)	62.50% (±1.97)	63.62% (±1.14)	62.63% (±1.21)
Sub11	45.50% (±3.59)	85.50% (±1.00)	88.25% (±1.27)	93.50% (±0.50)	37.33% (±1.96)	63.33% (±0.91)	62.83% (±2.91)	68.17% (±1.22)	27.37% (±3.35)	58.75% (±1.31)	58.37% (±2.07)	64.50% (±0.61)
Sub14	50.90% (±2.33)	99.50% (±0.52)	99.00% (±0.50)	99.50% (±0.07)	40.87% (±2.90)	95.33% (±0.85)	87.50% (±2.93)	95.83% (±0.52)	27.05% (±2.76)	84.25% (±1.21)	80.62% (±1.47)	88.13% (±1.04)
Sub15	54.20% (±3.61)	94.75% (±0.93)	94.00% (±0.93)	97.75% (±1.65)	39.67% (±1.51)	85.16% (±0.62)	77.33% (±1.70)	87.33% (±0.97)	29.90% (±2.36)	73.75% (±0.88)	73.37% (±2.15)	79.00% (±1.51)
Avg.	56.03%	92.51%	84.98%	94.80%	46.82%	78.63%	69.97%	81.62%	36.35%	66.47%	61.92%	71.05%
p	< 0.05	< 0.05	< 0.05		< 0.05	< 0.05	< 0.05		< 0.05	< 0.05	< 0.05	

prove that the clustering of features is well-grouped as the number of layers increases, as shown in Fig. 7.

C. Comparison of Classification Performance using FuDNN and Baseline Methods

Table II compares the classification performance between the FuDNN and conventional decoding methods. We used the common spatial pattern (CSP) [46], DeepConvNet [47], and EEGNet [48] as baseline methods to decode visual motion imagery data. We computed a non-parametric paired permutation test [51] to confirm the statistical differences between the classification results of the proposed method and the baseline methods. In the 2-class condition, we confirmed a high performance in deep learning-based methods, except for CSP, and there was a significant difference between the decoding methods ($P < 0.05$). The classification performances using the proposed method and DeepConvNet in the 2-class condition were recorded from 90.25% to 99.5%, with no significant variation between people and very stable performance. However, when we decoded the 3-class visual motion imagery data, there were some significant performance differences between the proposed method and baseline methods. When decoding the 3-class visual motion imagery data, the performance was the lowest with CSP, and the performance of DeepConvNet was slightly more dominant between the baseline methods using deep learning. In the 3-class condition, the classification performance of DeepConvNet was recorded as 63.33% to 95.33%, while the classification performance of EEGNet was recorded as 57.83% to 87.5%. For almost all subjects, we could see that performance using the proposed methods was higher than that using baseline methods, which resulted in statistically significant results ($p < 0.05$).

TABLE III
THE CLASSIFICATION PERFORMANCE UNDER LOSO CONDITION

	DeepConvNet [47]	EEGNet [48]	FuDNN
Sub4	38.13%	39.68%	39.50%
Sub6	33.13%	32.50%	40.13%
Sub9	51.38%	51.25%	51.25%
Sub14	58.25%	63.75%	61.88%
Sub15	44.00%	41.75%	50.25%
Avg.	44.98%	45.79%	48.60%

The differences in classification performance were more obvious when all classes were used. The average classification performance using the proposed network in this study was 71.05%, while EEGNet recorded 61.92% and DeepConvNet recorded 66.47%. As the class increases, we can confirm that the proposed method classifies EEG data more robustly than the baseline methods used. Overall, the classification performance showed a subject-dependent tendency regardless of class, which supports the notion that the proposed method is reasonable.

D. Classification Performance using Leave-One-Subject-Out Cross-Validation Approach

We applied the LOSO approach to verify the possibility of solving subject-independent issues. In the LOSO method, the network is trained using the data from the source subjects and

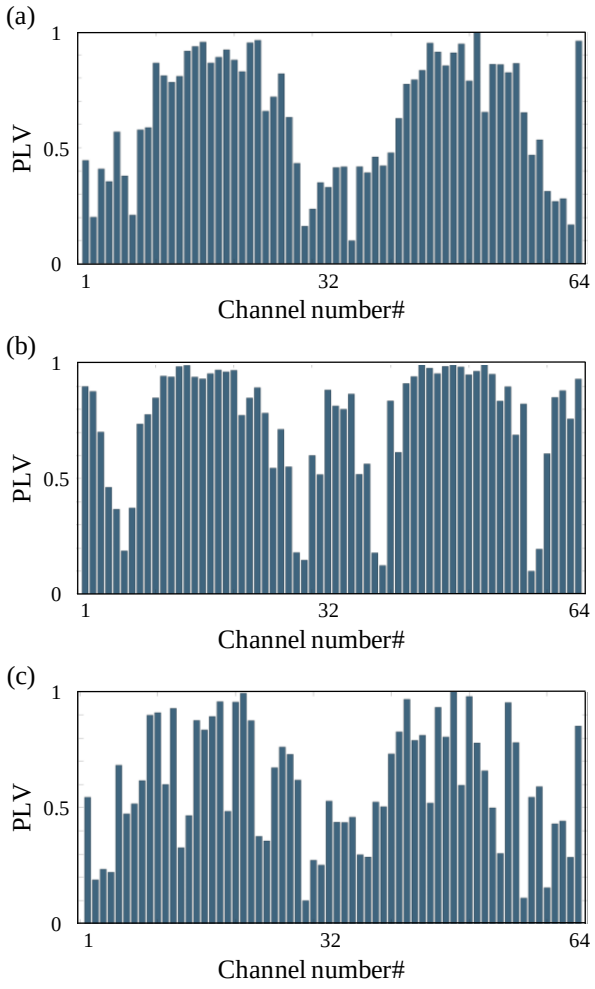

Fig. 9. Phase-locking value (PLV) representation in each channel of S6, S9, and S14. PLVs generally had a similar trend, which emphasizes that the raw electroencephalography signals have a similar tendency.

transferred to test the unknown data from the new subject. In this work, we set the training data to all subjects except one user who became a target. For a sufficient amount of training data, the sliding-window method was used as an augmentation method, such as classification in a subject-dependent condition. In LOSO conditions, baseline methods and proposed methods were trained using EEG data of 4 subjects, and a total of 3,200 training data were used, considering that the number of training data was 800 per subject. We selected the top five subjects who recorded high performance in the subject-dependent condition and confirmed the classification performance in the LOSO condition.

As shown in Table III, the proposed network recorded the highest average classification performance in the LOSO condition compared to the baseline methods. The proposed network had a 3.62% better performance than DeepConvNet and a 2.81% better performance than EEGNet. The classification performance of the proposed network in the LOSO condition was similar to that of the subject-dependent condition. However, unlike in the subject-dependent conditions,

TABLE IV
PEARSON CORRELATION COEFFICIENT SCORE FOR CALCULATING THE SIMILARITY OF PLV

	r-Value			
	Sub6	Sub9	Sub14	Sub15
Sub4	0.7488	0.8972	0.4726	-0.1817
Sub6		0.5625	0.6383	0.0663
Sub9			0.3528	-0.2657
Sub14				0.3090

EEGNet recorded a higher classification performance than DeepConvNet. The proposed network showed the strongest classification performance, regardless of these results. These results suggest that the proposed network is robust under subject-independent conditions.

IV. DISCUSSION

We provided the most intuitive BCI paradigm for subjects to improve EEG signal-decoding performance for the development of BCI applications. As a BCI paradigm, we provided 3D visual motion imagery to subjects in this study, and we performed data analysis to verify the quality of the EEG data obtained using our paradigm. The measurement of power spectra in the channels responsible for each brain region showed significant results in the prefrontal and occipital regions, indicating a similar tendency to conventional visual imagery related studies. That is, the EEG data collected from subjects are related to changes in brain signals when subjects perform visual motion imagery. ERSP results show that, when subjects imagine actions, meaningful signals are generated between 0.5 and 13 Hz, which includes the delta, theta, and alpha frequency ranges, which are associated with visual imagery. Furthermore, we can see from the ERSP results that the alpha wave is activated approximately 200 ms after the subject begins to imagine. We inferred that this phenomenon may be a characteristic of visual motion imagery, such as ERD/ERS, that occurs in motor imagery.

We also derived the classification performance of the proposed network compared with conventional deep learning approaches. As a result, the proposed network recorded higher performance in 2-class, 3-class, and 4-class conditions than the baseline method, and we could infer that the proposed network is an effective network for decoding visual motion imagery. There was a constant tendency between subjects among the deep learning networks, but there was no constant tendency between the proposed network and the CSP approach. Visual imagery is important in both spatial and temporal information, which results in lower classification performance for the CSP approach that does not emphasize temporal information, thereby eliminating the constant tendency between subjects. In addition, there were subjects with higher performance than the proposed network (Sub8, Sub4) in 2- and 3-class conditions, respectively. However, these results were not considered significant because there was no significant difference in classification performance and they had a higher performance than the average performance.

Because visual motion imagery data are based on the user's imagining temporal changes in a 3D space, we designed the proposed network based on this. The network proposed in this study emphasized channels containing meaningful features related to visual motion imagery based on PLVs and used them to modify the raw EEG data. In addition, the channel-wise separable convolution layer was placed on the last layer of the CNN, features were extracted using the two preceding convolution layers to contain spatial information, and these features were used as inputs to BiLSTM. This structure extracts information based on features, including spatial information when extracting temporal features of the input using BiLSTM, so the output contains both temporal and spatial information.

We conducted an ablation study to verify the efficiency of the proposed network. As a result, the more we used the overall structure of the proposed network to decode EEG data, the more obvious the clustering distribution of the output features. However, in the case of PP and OD, even though the entire network was used, the distribution of features was not completely separated. In particular, in the case of the OD class, it can be seen that the distribution is very widely distributed, which means that data have not been properly learned. Considering that the distribution of data of other classes except OD is narrowly distributed, these results were interpreted as characteristics of the data corresponding to the OD class.

As a result, for all subjects, all deep learning approaches recorded a classification performance of 25% or more, which is the chance level, and among them, the proposed network recorded the highest performance. The reason visual motion imagery is possible in a subject-independent approach is that it has a constant data distribution regardless of the subject, and the spatial area to be emphasized in the network is almost similar. As a result of calculating the PLV when the subject performed visual motion imagery (Fig. 9), there was a tendency to have similar PLVs for each channel. In other words, because similar PLVs are derived from spatially similar channels, we can infer the possibility of a subject-independent approach. As shown in Table IV, the similarity of PLVs among the subjects was calculated using the Pearson correlation coefficient (CC) r, which refers to the similarity of PLVs between subjects, and mostly indicates values above 0.3 with a distinct amount of correlation. Because most users have PLVs with distinct correlations, based on this, we can infer that users are imagining in a similar way, which could be the starting point for development to the subject-independent approach. All three cases with r lower than 0.3 were related to Sub15, which allows us to infer that Sub15 had a different pattern of imagination from other subjects. If re-learning is requested from these types of subjects or a deep learning approach that minimizes spatial information is applied, better performance can be expected. In this work, we construct a network where spatial information is emphasized based on PLVs, which can be used as an indicator of data learning in subject-independent conditions.

V. Conclusions and Future Works

In this paper, we propose a 3D-BCI training platform for users to perform visual motion imagery effectively. Using the 3D-BCI training platform, we were able to collect high-quality visual motion imagery data from participants, and we verified the quality of the data using neurophysiological methods. In addition, we proposed a FuDNN to decode the obtained visual motion imagery data. The network was designed to consider both spatial and temporal information based on the characteristics of visual motion imagery. Using functional connectivity, we emphasized channels that are highly correlated with visual motion imagery, and based on this, we extracted spatial information using convolution layers. Subsequently, we used the extracted features as inputs to BiLSTM. The network proposed in this study recorded a robust decoding performance regardless of the number of classes. It is important to record high classification performance for various classes, but it is also significant that the types of classes proposed in this paper were designed with complex upper-limb movements.

In future work, we will develop a FuDNN for high classification performance so that it can be applied to real-time BCI scenarios. In addition, we will explore methods to lighten the networks proposed in this study to reduce the computational complexity. We plan to collect data by increasing the number of classes to decode more diverse upper-limb movements. Based on this, we will apply the proposed network to an EEG-based robotic arm system and contribute to the development of rehabilitation systems for patients with tetraplegia or supporting the daily life activities of healthy people.

Acknowledgment

The authors thank J.-H. Cho and B.-H. Lee for their help with the dataset construction and for useful discussions.

References

[1] T. M. Vaughan, W. J. Heetderks, L. J. Trejo, W. Z. Rymer, M. Weinrich, M. M. Moore, A. Kübler, B. H. Dobkin, N. Birbaumer, E. Donchin, E. W. Wolpaw, J. R. Wolpaw, "Brain-computer interface technology: A review of the second international meeting," *IEEE Trans. Neural Syst. Rehabil. Eng.*, vol. 11, no. 2, pp. 94–109, Jun. 2003.

[2] J. Meng, S. Zhang, A. Bekyo, J. Olsoe, B. Baxter and B. He, "Non-invasive electroencephalogram based control of a robotic arm for reach and grasp tasks," *Sci. Rep*, vol. 6, p. 38565, 2016.

[3] R. Leeb, L. Tonin, M. Rohm, L. Desideri, T. Carlson, and J. d. R. Millan, "Towards independence: a BCI telepresence robot for people with severe motor disabilities," *Proc. IEEE*, vol. 103, no. 6, pp. 969–982, 2015.

[4] H.-I. Suk and S.-W. Lee, "A novel bayesian framework for discriminative feature extraction in brain-computer interfaces," *IEEE Trans. Pattern Anal. Mach. Intell.*, vol. 35, no. 2, pp. 286–299, 2012.

[5] K. K. Ang and C. Guan, "EEG-based strategies to detect motor imagery for control and rehabilitation," *IEEE Trans. Neural Syst. Rehabil. Eng.*, vol. 25, no. 4, pp. 392–401, 2016.

[6] N.-S. Kwak, K.-R. Müller, and S.-W. Lee, "A lower limb exoskeleton control system based on steady state visual evoked potentials," *J. Neural Eng.*, vol. 12, no. 5, p. 056009, 2015.

[7] Z. Zhang and Y. Huang and S. Chen and J. Qu and X. Pan and T. Yu and Y. Li, "An intention-driven semi-autonomous intelligent robotic system for drinking," *Front. Neurorobot.*, vol. 48, no. 11, pp. 1–14, 2017.

[8] K.-T. Kim, H.-I. Suk, and S.-W. Lee, "Commanding a Brain-Controlled Wheelchair Using Steady-State Somatosensory Evoked Potentials," *IEEE Trans. Neural Syst. Rehabil. Eng.*, vol. 26, no. 3, pp. 654–665, 2018.

[9] M.-H. Lee, J. Williamson, D.-O. Won, S. Fazli, and S.-W. Lee, "A high performance spelling system based on EEG-EOG signals with visual feedback," *IEEE Trans. Neural Syst. Rehabil. Eng.*, vol. 26, no. 7, pp. 1443–1459, 2018.

[10] J.-H. Jeong, K.-H. Shim, J.-H. Cho, and S.-W. Lee, "Trajectory decoding of arm reaching movement imageries for brain–controlled robot arm system," in *Conf. Proc. IEEE Eng. Med. Biol. Soc. (EMBC)*, 2019, pp. 23–27.

[11] J.-H. Kim, and F. Bießmann, and S.-W. Lee, "Decoding three-dimensional trajectory of executed and imagined arm movements from electroencephalogram signals," *IEEE Trans. Neural Syst. Rehabil. Eng.*, vol. 23, no. 5, pp. 867–876, 2014.

[12] N. Houmani, F. Vialatte, E. Gallego-Jutglà, G. Dreyfus, V.-H. Nguyen-Michel, J. Mariani, and K. Kinugawa, "Diagnosis of alzheimer's disease with electroencephalography in a differential framework," *PloS ONE*, vol. 13, no. 3, p. e0193607, 2018.

[13] U. R. Acharya, S. L. Oh, Y. Hagiwara, J. H. Tan, and H. Adeli, "Deep convolutional neural network for the automated detection and diagnosis of seizure using EEG signals," *Comput. Biol. Med*, vol. 100, pp. 270–278, 2018.

[14] J.-H. Cho, J.-H. Jeong, K.-H. Shim, and S.-W. Lee, "Classification of various grasping tasks based on temporal segmentation method using EEG and EMG signals." in *GBCIC*, 2019.

[15] R. Foong, K. K. Ang, C. Quek, C. Guan, K. S. Phua, C. W. K. Kuah, V. A. Deshmukh, L. H. L. Yam, D. K. Rajeswaran, N. Tang *et al.*, "Assessment of the efficacy of EEG-based MI-BCI with visual feedback and EEG correlates of mental fatigue for upper-limb stroke rehabilitation," *IEEE Trans. Biomed.*, vol. 67, no. 3, pp. 786–795, 2019.

[16] R. Chai, S. H. Ling, G. P. Hunter, Y. Tran, and H. T. Nguyen, "Brain–computer interface classifier for wheelchair commands using neural network with fuzzy particle swarm optimization," *IEEE J. Biomed. Health Inform.*, vol. 18, no. 5, pp. 1614–1624, 2013.

[17] J.-H. Jeong, K.-H. Shim, D.-J. Kim, and S.-W. Lee, "Brain-controlled robotic arm system based on multi-directional CNN-BiLSTM network using EEG signals," *IEEE Trans. Neural Syst. Rehabil. Eng.*, vol. 28, no. 5, pp. 1226–1238, 2020.

[18] V. Mihajlović, B. Grundlehner, R. Vullers, and J. Penders, "Wearable, wireless EEG solutions in daily life applications: what are we missing?" *IEEE J. Biomed. Health Inform.*, vol. 19, no. 1, pp. 6–21, 2014.

[19] C. I. Penaloza and S. Nishio, "BMI Control of a Third Arm for Multitasking," *Sci. Robot.*, vol. 3, no. 20, pp. 1–6, 2018.

[20] B. He, B. Baxter, B. J. Edelman, C. C. Cline, and W. Y. Wenjing, "Non-invasive brain-computer interfaces based on sensorimotor rhythms," *Proc. IEEE*, vol. 103, no. 6, pp. 907–925, 2015.

[21] D. Zhang, K. Chen, D. Jian, and L. Yao, "Motor imagery classification via temporal attention cues of graph embedded EEG signals," *IEEE J. Biomed. Health. Inform.*, vol. 24, no. 9, pp. 2570–2579, 2020.

[22] M. Arvaneh, C. Guan, K. K. Ang, and C. Quek, "Optimizing spatial filters by minimizing within-class dissimilarities in electroencephalogram-based brain–computer interface," *IEEE Trans. Neural Netw. Learn. Syst.*, vol. 24, no. 4, pp. 610–619, 2013.

[23] F. Lotte, "Signal processing approaches to minimize or suppress calibration time in oscillatory activity-based brain–computer interfaces," *Proc. IEEE*, vol. 103, no. 6, pp. 871–890, 2015.

[24] S. Saha, K. I. U. Ahmed, R. Mostafa, L. Hadjileontiadis, and A. Khandoker, "Evidence of variabilities in EEG dynamics during motor imagery-based multiclass brain–computer interface," *IEEE Trans. Neural Syst. Rehabil. Eng.*, vol. 26, no. 2, pp. 371–382, 2017.

[25] A. M. Azab, L. Mihaylova, K. K. Ang, and M. Arvaneh, "Weighted transfer learning for improving motor imagery-based brain-computer interface," *IEEE Trans. Neural Syst. Rehabil. Eng.*, vol. 27, no. 7, pp. 1352–1359, 2019.

[26] B.-H. Kwon, J.-H. Jeong, J.-H. Cho, and S.-W. Lee, "Decoding of intuitive visual motion imagery using convolutional neural network under 3d-bci training environment," in *2020 IEEE International Conference on Systems, Man, and Cybernetics (SMC)*. IEEE, 2020, pp. 2966–2971.

[27] K. Koizumi, K. Ueda, N. Tateyama, and M. Nakao, "EEG source analysis of visual motion imagery for application to brain-computer interface." in *GBCIC*, 2019.

[28] T. Sousa, C. Amaral, J. Andrade, G. Pires, U. J. Nunes, and M. Castelo-Branco, "Pure visual imagery as a potential approach to achieve three classes of control for implementation of BCI in non-motor disorders," *J. Neural Eng.*, vol. 14, no. 4, p. 046026, 2017.

[29] C. J. Honey, O. Sporns, L. Cammoun, X. Gigandet, J.-P. Thiran, R. Meuli, and P. Hagmann, "Predicting human resting-state functional connectivity from structural connectivity," *Proc. Natl. Acad. Sci. U.S.A.*, vol. 106, no. 6, pp. 2035–2040, 2009.

[30] J.-P. Lachaux, E. Rodriguez, J. Martinerie, and F. J. Varela, "Measuring phase synchrony in brain signals," *Hum. Brain Mapp.*, vol. 8, no. 4, pp. 194–208, 1999.

[31] B. J. Roach and D. H. Mathalon, "Event-related EEG time-frequency analysis: an overview of measures and an analysis of early gamma band phase locking in schizophrenia," *Schizophr. Bull.*, vol. 34, no. 5, pp. 907–926, 2008.

[32] C.-R. Phang, F. Noman, H. Hussain, C.-M. Ting, and H. Ombao, "A multi-domain connectome convolutional neural network for identifying schizophrenia from EEG connectivity patterns," *IEEE J. Biomed. Health Inform.*, vol. 24, no. 5, pp. 1333–1343, 2019.

[33] S. U. Amin, M. Alsulaiman, G. Muhammad, M. A. Mekhtiche, and M. S. Hossain, "Deep learning for EEG motor imagery classification based on multi-layer cnns feature fusion," *Future Gener. Comput. Syst.*, vol. 101, pp. 542–554, 2019.

[34] Y. Yuan, G. Xun, K. Jia, and A. Zhang, "A multi-view deep learning framework for EEG seizure detection," *IEEE J. Biomed. Health Inform.*, vol. 23, no. 1, pp. 83–94, 2018.

[35] X. Xing, Z. Li, T. Xu, L. Shu, B. Hu, and X. Xu, "SAE+LSTM: A new framework for emotion recognition from multi-channel EEG," *Front. Neurorobot.*, vol. 13, p. 37, 2019.

[36] P. Zhang, X. Wang, W. Zhang, and J. Chen, "Learning spatial–spectral–temporal EEG features with recurrent 3D convolutional neural networks for cross-task mental workload assessment," *IEEE Trans. Neural Syst. Rehabil. Eng.*, vol. 27, no. 1, pp. 31–42, 2018.

[37] Y. Jiao, Y. Deng, Y. Luo, and B.-L. Lu, "Driver sleepiness detection from EEG and EOG signals using GAN and LSTM networks," *Neurocomputing*, 2020.

[38] D.-A. Clevert, T. Unterthiner, and S. Hochreiter, "Fast and accurate deep network learning by exponential linear units (elus)," *arXiv preprint arXiv:1511.07289*, 2015.

[39] L.-C. Chen, Y. Zhu, G. Papandreou, F. Schroff, and H. Adam, "Encoder-decoder with atrous separable convolution for semantic image segmentation," in *Proc. Eur. Conf. Comput. Vis.*, 2018, pp. 801–818.

[40] F. Chollet, "Xception: Deep learning with depthwise separable convolutions," in *Proc. IEEE Conf. Comput. Vis. Pattern Recognit.*, 2017, pp. 1251–1258.

[41] A. Graves and J. Schmidhuber, "Framewise phoneme classification with bidirectional lstm and other neural network architectures," *Neural Netw.*, vol. 18, no. 5-6, pp. 602–610, 2005.

[42] A. Graves, N. Jaitly, and A.-R. Mohamed, "Hybrid speech recognition with deep bidirectional lstm," in *Proc. IEEE Workshop Autom. Speech Recognit. Understand. (ASRU)*. IEEE, 2013, pp. 273–278.

[43] B. Blankertz, M. Tangermann, C. Vidaurre, S. Fazli, C. Sannelli, S. Haufe, C. Maeder, L. E. Ramsey, I. Sturm, G. Curio, and K.-R. Müller, "The Berlin brain-computer interface: non-medical uses of BCI technology," *Front. Neurosci.*, vol. 4, p. 198, Dec. 2010.

[44] A. Delorme and S. Makeig, "EEGLAB: an open source toolbox for analysis of single-trial EEG dynamics including independent component analysis," *J. Neurosci. Methods*, vol. 134, no. 1, pp. 9–21, Mar. 2004.

[45] S. Makeig, "Auditory event-related dynamics of the EEG spectrum and effects of exposure to tones," *Electroencephalogr. Clin. Neurophysiol.*, vol. 86, no. 4, pp. 283–293, 1993.

[46] K. K. Ang, Z. Y. Chin, C. Wang, C. Guan, and H. Zhang, "Filter bank common spatial pattern algorithm on BCI competition IV datasets 2a and 2b," *Front. Hum. Neurosci.*, vol. 6, p. 39, Mar. 2012.

[47] R. T. Schirrmeister, J. T. Springenberg, L. D. J. Fiederer, M. Glasstetter, K. Eggensperger, M. Tangermann, F. Hutter, W. Burgard, and T. Ball, "Deep learning with convolutional neural networks for EEG decoding and visualization," *Hum. Brain Mapp.*, vol. 38, no. 11, pp. 5391–5420, 2017.

[48] V. J. Lawhern, A. J. Solon, N. R. Waytowich, S. M. Gordon, C. P. Hung, and B. J. Lance, "EEGNet: A compact convolutional neural network for EEG-based brain-computer interfaces," *J. Neural Eng.*, vol. 15, no. 5, pp. 1–17, 2018.

[49] H. Jebelli, M. M. Khalili, and S. Lee, "A continuously updated, computationally efficient stress recognition framework using electroencephalogram (EEG) by applying online multitask learning algorithms (omtl)," *IEEE J. Biomed. Health Inform.*, vol. 23, no. 5, pp. 1928–1939, 2018.

[50] A. Arsalan, M. Majid, A. R. Butt, and S. M. Anwar, "Classification of perceived mental stress using a commercially available EEG headband," *IEEE J. Biomed. Health Inform.*, vol. 23, no. 6, pp. 2257–2264, 2019.

[51] E. Maris and R. Oostenveld, "Nonparametric statistical testing of EEG- and MEG-data," *J. Neurosci. Methods.*, vol. 164, no. 1, pp. 177–190, Aug. 2007.